Damage identification and localisation using changes in modal parameters for civil engineering structures

J. Mahowald[1], S. Maas[1], D. Waldmann[1], A. Zuerbes[2], F. Scherbaum[1]
[1] University of Luxembourg, Faculty of Science, Technology and Communication, Luxembourg
6, rue Richard Coudenhove-Kalergi
L-1359 Luxembourg, Luxembourg
e-mail: **jean.mahowald@uni.lu**

[2] Fachhochschule Bingen, Fachbereich 2
Berlinstrasse 109
D-55411 Bingen, German

Abstract
In this paper dynamic testing of some civil engineering structures is presented. The investigated objects are prestressed and non-prestressed industrially produced concrete slab elements under laboratory conditions, as well as an in situ prestressed concrete bridge. In order to achieve damage assessment, different analyses based on modal parameters changes are done. To this end, the structures are artificially damaged by cutting locally their passive or prestressed steel reinforcement. Moreover, to cause cracks, the structures are loaded with a varying experimental mass. For modal analysis all objects are excited sinusoidally by an electrodynamic shaker in the laboratory and by special exciters in the case of the bridge. In this article, a set of modal parameters, i.e. eigenfrequencies and modes shapes are determined and compared according the damage states. It results that the shift of the eigenfrequencies is a valuable damage indicator whereas the modeshapes variations are small and more difficult to interpret. Further, the modal parameters are used to calculate the flexibility, i.e. the inverse stiffness matrix and their changes revealing clear differences according to the damage at the correct locations. In addition, the mode shape slope and curvature, as well as the bending and strain fractional energy method for the bridge are presented, indicating the loss of stiffness and hence the damage.

1 Introduction

The overall goal of the investigated civil engineering structures is the usability of dynamic methods for damage assessment. First under laboratory conditions, tests are conducted in order to simulate bridges and to see the feasibility of such testing for condition control. Further, a 102m span bridge is under strong investigation to reveal the possible use on in situ objects identifying and even localising damage in civil structures. The advantage of dynamic methods is that they are easy manageable and not very time consuming in contrast to visual inspections, often used for condition control and inspections on bridges for example. The changes of the eigenfrequencies, as well as the changes in the flexibility matrices are known as trustful indicators for damage assessment, whereas the eigenfrequencies yield only information on damage detection ([1], [2]) in contrast to the flexibility matrices which reveal also indication on the localisation of a damage ([3], [4]). Moreover, the slope, the curvature and the bending and strain fractional energy methods show also their potential for damage assessment on beams and bridges ([5], [6], [7], [8]) and could therefore also be suitable for the presented structures under artificial damage states. Hence, in this paper these methods are presented and compared for each other for possible damage assessment.

1.1 Objects and damage scenarios

1.1.1 Reinforced and prestressed slabs

The investigated panels are manufactured by ECHOLUX, subsidiary of ECHO placed in Luxembourg, and are of type VSF-15-120. They are made of concrete C50/60 with a measured average compressive strength of 58.3 N/mm^2 (quality control of manufacturer). The quality of the reinforcement is St1470/1670 and the corresponding elastic modulus 205000 N/mm^2. In the upper section of the panel 4 wires are placed with a diameter of 5 mm and in the lower section 12 wires with a diameter of 7 mm. Figure 1 shows the cross section of the concrete slabs with the reinforcement in the upper and lower part. For our test purposes, two slabs are under investigation: a prestressed concrete slab (PC) and for the University of Luxembourg a special manufactured reinforced slab (RC) without any prestress.

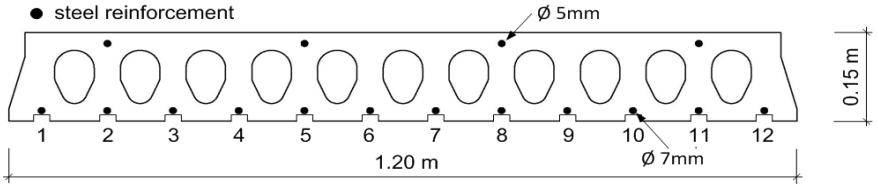

Figure 1: Cross-section of the panels with the reinforcement in the upper and lower part of the slab. At the bottom at half length the concrete was removed to have access to the steel wires for cutting.

For the artificial damage, the tendons in the lower part of the panels are cut successively with a flame cutter. For this, holes in the middle on the slab, in section C on Figure 2 are drilled (sketch on Figure 1). The different damage states with the percentage of locally reduced pretension, respectively reinforcement are illustrated on Table 1. According to the different damage states, and after loading of 4 steel weights, with a force of 33.4kN, cracks occurred in the slabs represented schematically on Figure 3.

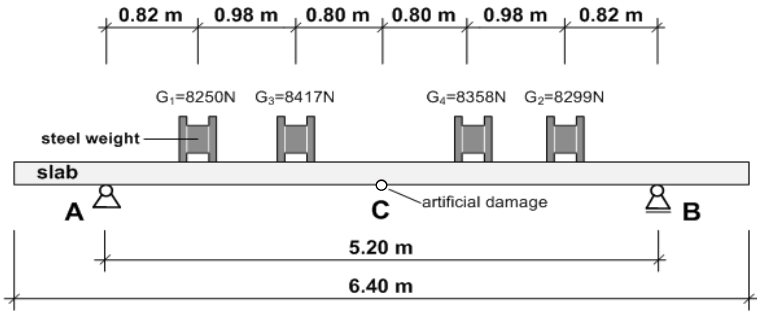

Figure 2: View of the slab from the side with the dimensions and places of the weights (G1, G2, G3 and G4) as well as the axes of the bearings (A and B) and C the middle of the distance between the supports.

no.	damage scenario	location	Percentage: cut cables	additional loads
#0	initial state: undamaged	-	-	4 and 0* weights
#1	cutting of tendon no.: 6, 7	axis C	16.7 %	4 and 0* weights
#2	cutting of tendon no.: 6, 7, 2, 11	axis C	33.3 %	4 and 0* weights
#3	cutting of tendon no.: 6, 7, 2, 11, 4, 9	axis C	50.0 %	4 and 0* weights
#4	cutting of tendon no.: 6, 7, 2, 11, 4, 9, 3, 10	axis C	66.7 %	4 and 0* weights

Table 1: Damage scenarios and load cases for the prestressed slab (PC) and for the presented tests special manufactured reinforced slab (RC) (* represents the dynamic measurements after the slab was loaded with an additional load of 4 steel weights)

One can clearly recognise that for the reinforced slab (RC), the crack formation is completed after loading with 4 steel weights in the intact state #0. For the higher damage states, when cutting further reinforcement, the cracks grow. For the prestressed slab (PC), a first small hairline crack occurs for damage state #2 after loading with 4 steel weights, and rises when cutting more tendons for damage state #3. For both slabs, collapse arrived at damage state #4 after loading with 4 steel weights.

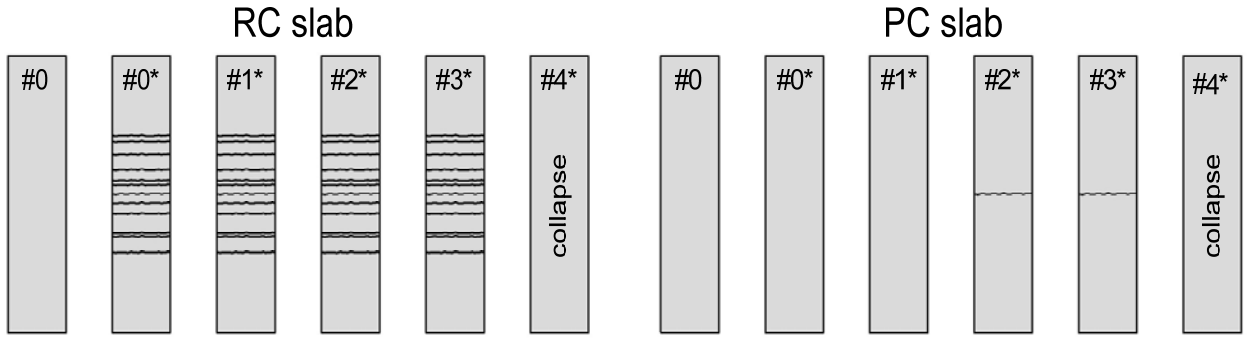

Figure 3: Progressive cracking of the RC slab (left) and the PC slab (right) between scenarios #0 and #4 (* represents the states after an additional load of 4 steel weights)

1.1.2 Bridge Champangshiehl

The in situ object, the bridge Champangshiehl (Figure 4), was built from 1965 to 1966 and connects the centre of Luxembourg with the district Kirchberg. It is a two span prestressed concrete bridge with different span length. The length of the bridge is 102 m, divided into two fields of 65 m and 37 m in length. The superstructure of the bridge is a prestressed box girder with 32 parabolic, 24 upper straight lined and 20 lower straight lined subsequently grouted tendons (Figure 5). The roadbed has a width of 12.5 m and the box girder of 6.5 m with a height of 2.62 m, as illustrated on Figure 4. The bridge is made of concrete B450 and the tendons of Steel ASTM A.416 57T. The superstructure is supported by two abutments and one column made of reinforced concrete. At the west abutment (abutment of the large field) is a floating bearing made of a steel roll, whereas on the east abutment, the bearing is fixed. Between the superstructure and the substructure over the pylon an elastomeric support is placed. In 1987, 56 external prestressed steel cables were added into the box girder of the large field due to additional safety considerations [9].

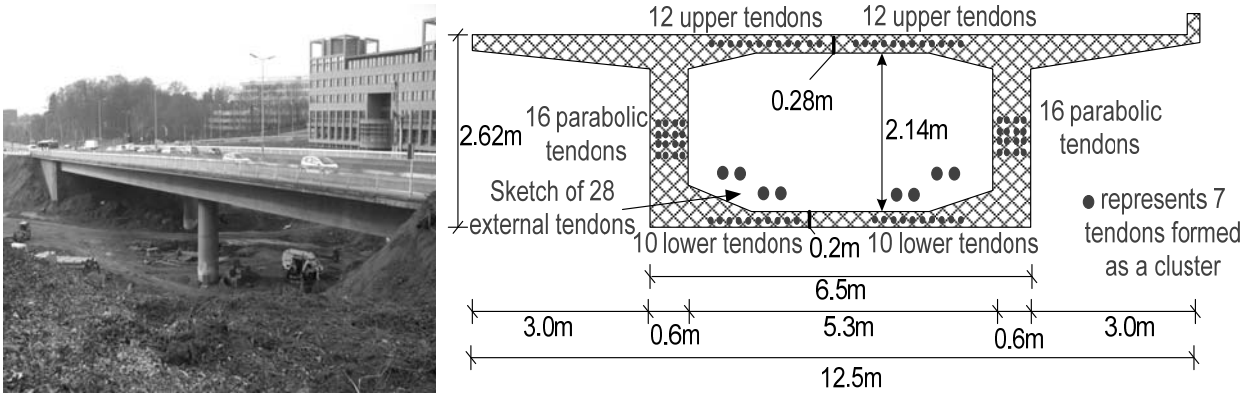

Figure 4: Picture of the bridge in winter 2010 (left); the cross section with all the tendons (right).

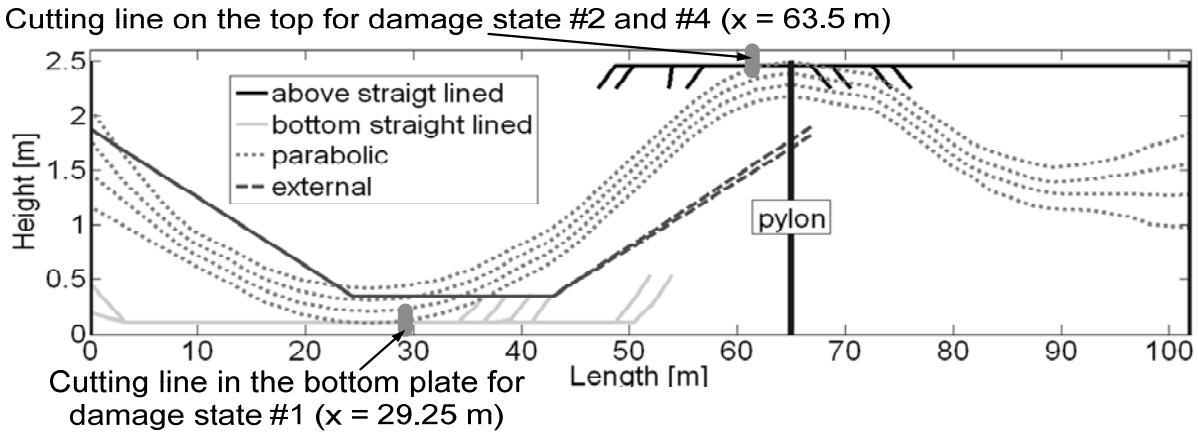

Figure 5: Longitudinal section of the bridge showing the different types of tendons and the cutting sections.

In order to validate the presented testing methods for damage assessment, tests are conducted, like for the slabs, also for different damage scenarios. Table 2 summarises the different damage states (intact #0 to the most damaged #4) by continuously cutting a defined number of tendons at two different sections of the bridge, as illustrated on Figure 5 and Table 2. As for both types of structures the damage states are crucial to evaluate the sensitivity of the tests according the severity of introduced damage and formation of cracks, also for the bridge cracks occurred at the different damage states when loaded with an additional experimental mass. This is achieved by 38 beam blanks from ArcelorMittal with a total mass of 245 t. The formation of cracks for the different damage state are summarised on Table 3 and schematically shown on Figure 6.

Damage state	Cutting tendons	Percentage cutting (100% equals all tendons in the defined section)	
		x=29.25 m	x=63.5 m
# 0	Undamaged state	0%	0%
# 1	20 straight lined tendons in the lower part of the bridge (x=29.25 m)	33.7%	0%
# 2	8 straight lined tendons in the upper part of the bridge over the pylon (x=63.5 m)	33.7%	12.6%
# 3	56 external tendons	46.1%	24.2%
# 4	16 straight lined and 8 parabolic tendons in the upper part of the bridge (x=63.5 m)	46.1%	62.12%

Table 2: Description of the damage scenarios according to the cutting sections shown on Figure 5.

Damage state	Crack description
#1	Shear cracks due to the new anchorage points of the prestressed cables by cutting the lower 20 straight lined prestressed cables (black cracks, dashed line on Figure 6)
#1-Loaded	#1 + one crack in the girder at the north side up to 1.5m from the bottom line (dark grey cracks, solid line on Figure 6) and 1m on the south side at the cutting line of the lower 20 straight lined tendons
#3	#1-Loaded + growing of the existing cracks and formation of new cracks at 0.45L (grey cracks, dashed line on Figure 6) + small crack between the holes on the upper side with loading (Figure 6)
#4	#3 + crack above the pylon (grey cracks, solid line on Figure 6)

Table 3: Description of the appearance of cracks according to the damage states and mass.

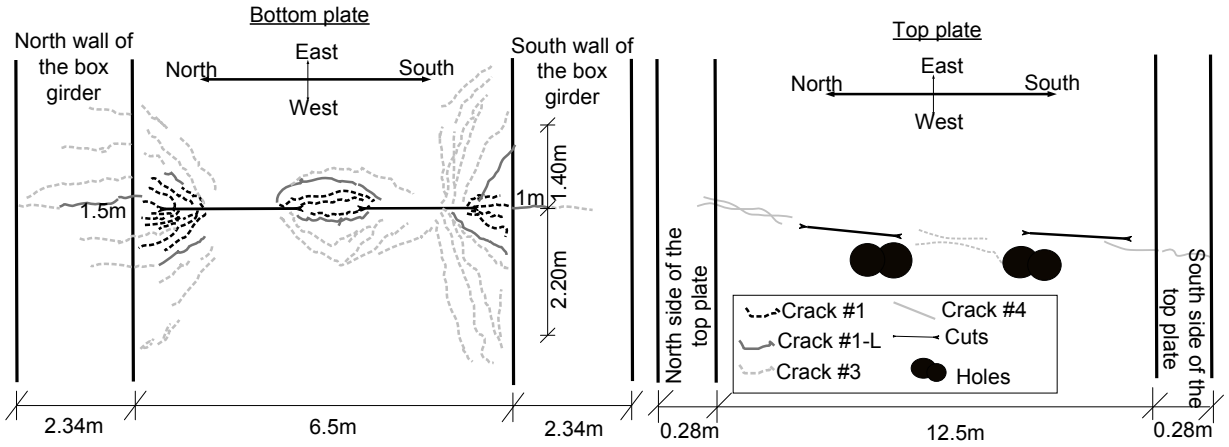

Figure 6: Schematic view of the crack appearance at the bottom plate around the cutting line at x=29.25m (left) and on the top plate around the cutting line x=63.5m (right)

2 Testing procedures

In this chapter, the experimental setups are presented. In contrast to the investigations already made on the presented structures in previous work [2], [4], the modeshapes are evaluated using a coarse grid of transducer position ending in a wider resolution.

2.1 Experimental setup

The dynamic parameters, for both structures are measured using a defined number of accelerometers. For the bridge Champangshiehl, 20 accelerometers (of type PCB 393B04 with a sensitivity of approx: 1000mV/g) are set according Figure 7 capturing the responses of the bridge due to a well known excitation force. For the slabs, only 10 transducers were installed and set according Figure 8. For the structures one additional transducer is put near the exciters as a driving point for modal analysis. As already mentioned, in this paper only the results from the coarse grid for both type of structures are presented, with a force excitation of 2500N (unbalanced mass exciter) for the bridge Champangshiehl and 100N (electromagnetic shaker of type TIRA 2.7kN) for the slabs. Other data with different forces and dense measurement grids can be read in further literature [2]. The data are processed by Mescope software using the global polynomial method to retrieve mass normalised mode shapes. The data is acquired with 2000Hz for the slabs and 1000Hz for the bridge Champangshiehl. The sweep rate for the slabs is 0.1Hz/s and runs from 3Hz to 150Hz and for the bridge Champangshiehl of 0.02Hz/s from 1Hz to 20Hz.

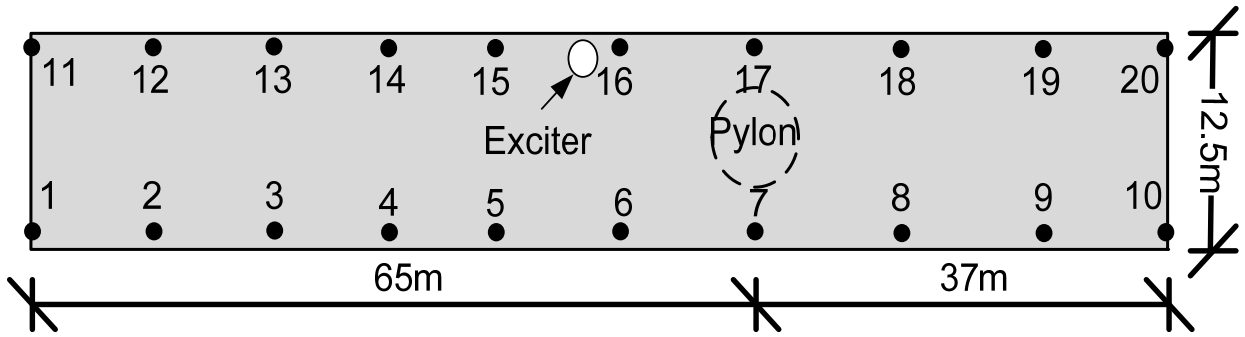

Figure 7: Measurement setup for the dynamic tests with the accelerometers positions (black) and exciter position (white) for the bridge Champangshiehl.

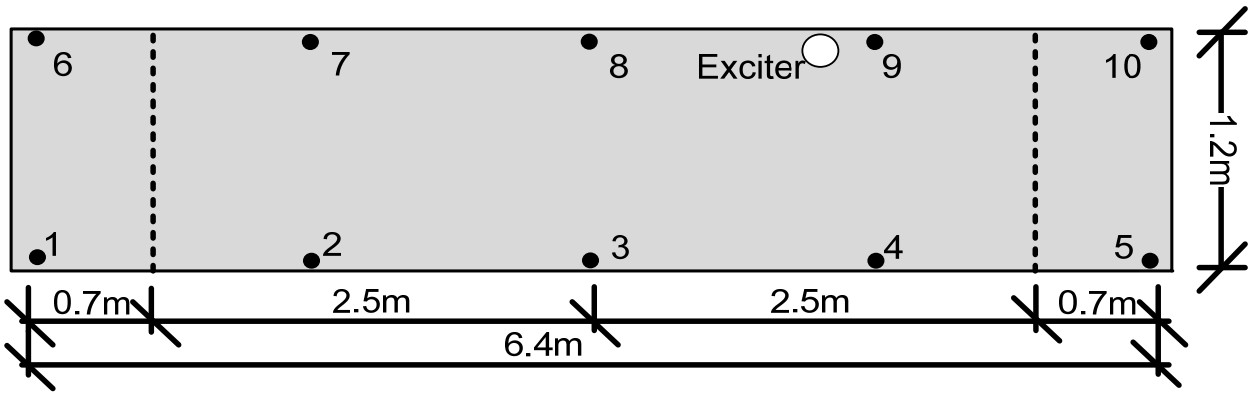

Figure 8: Measurement setup for the dynamic tests with the accelerometers positions (black) and exciter position (white) for the concrete slabs.

3 Results

3.1 Eigenfrequencies and Modeshapes

In the following, the changes in modal parameters, i.e. the eigenfrequencies and modeshapes are discussed. When the structure is changed by cracks for example the bending stiffness EI varies also resulting by a decrease of the eigenfrequencies. These changes mentioned by the relative decrease to the intact states and their corresponding modeshapes are presented on the following figures. For better visualisation on the modeshapes, both sides of the structures are plotted in one graph, the side of the structure with no excitation position on the left (transducer position 1 to 5 for the slabs and 1 to 10 for the bridge Champangshiehl) and the excitation side on the right (transducer position 6 to 10 for the slabs and 11 to 20 for the bridge Champangshiehl). One has to add, that only some modes are presented which are predominant on the Frequency response functions, and, therefore, detectable for each damage states and comparable to the intact state.

3.1.1 Reinforced and prestressed concrete slabs

For the reinforced and prestressed concrete slabs, different behaviours are noticed for the changes in eigenfrequencies and modeshapes. Regarding first the reinforced slab, one can see on Figure 9 that the eigenfrequencies decreases according the different damage states, which is also expected. From the intact state #0 to damage state #0* obvious changes are noticed. This is due to the fact, that the crack pattern is already completed due to the loading of the 4 steel weights. These cracks change the bending stiffness resulting in a reduction of the eigenfrequencies. First a decrease of 22.9% is recognised for the first eigenfrequency B1 (B stands for bending mode and T for Torsional mode) for damage state #0* With increasing damage, i.e. cutting of reinforcement, the cracks grow explaining the continuous reduction of the eigenfrequencies for the other damage states, up to 36.2% for damage state #3*. For mode T1 and B2, the frequencies also decrease, but only with 22.9% and 22.4% respectively. Thus, regarding only the eigenfrequencies for the reinforced slab, the changes according the damage, i.e. the formation of cracks are obvious and, thus, represent a trustful indicator for a changed structure. Considering the modeshapes, also changes are noticed; however an overall pattern of these changes according the damage states is not detectable.

On the other hand, considering the prestressed slab, first when unloaded on Figure 10, no crucial decrease of the eigenfrequencies according the damage like for the reinforced slab can be recognised. Only changes up to 3.4% for the first eigenfrequency B1 and up to 8.6% for the mode T2 are identified. As already denoted in [2], the cracks, once formed in the slab, are closed due to the pretension force and so no changes in the bending stiffness are noticed. Here the changes on the modeshapes are even minor for B1

and T1 and for B2 and T2 neither a valuable pattern is recognised, making the variations on the modeshapes difficult to interpret.

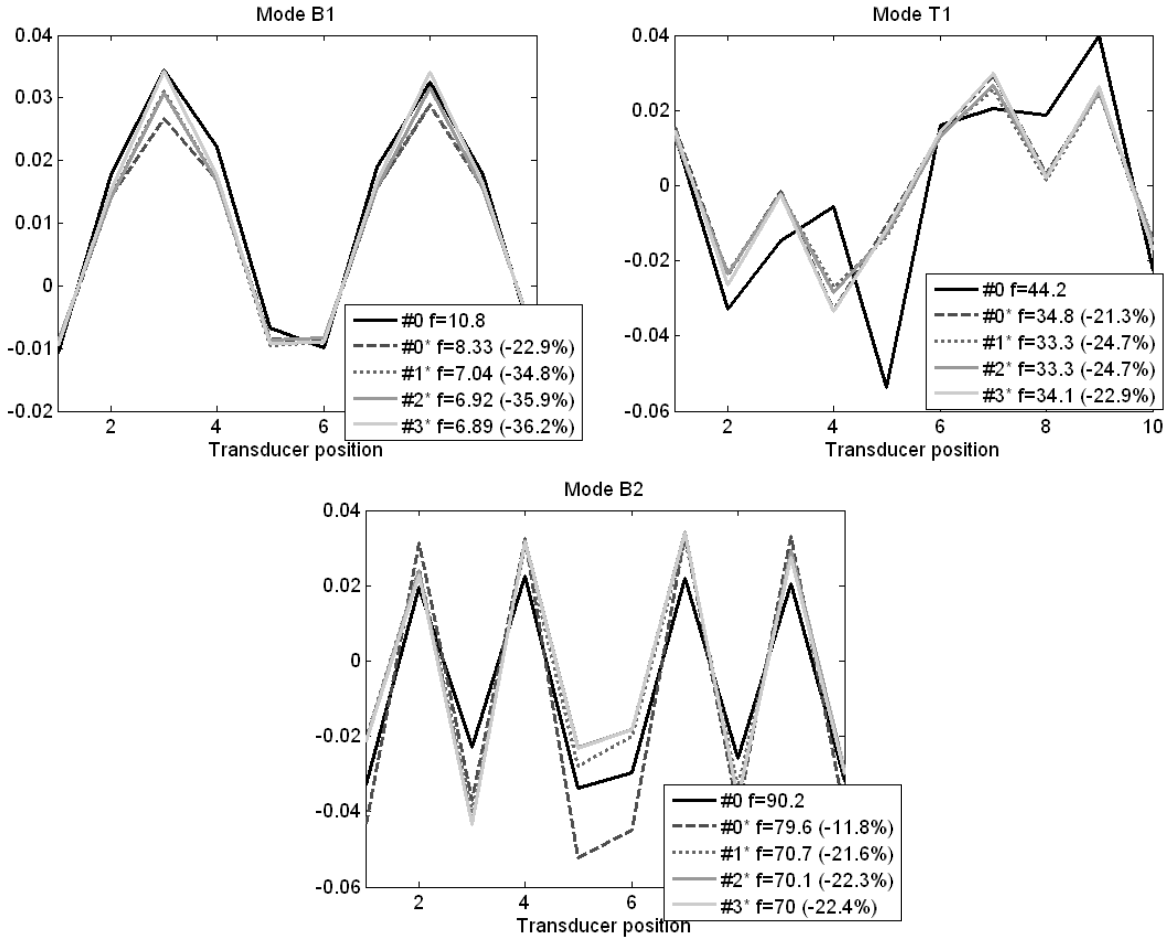

Figure 9: Eigenfrequencies and modeshapes of the reinforced slab (RC).

To open the cracks of the prestressed slabs, these are loaded with an experimental mass of 3340kg. As for damage state #1-L (L stands for loaded) no cracks occurred, also no crucial changes can be recognised on the first eigenfrequency B1 on Figure 11. Regarding damage state #2-L and #3-L a continuous decrease is seen, concluding in changes of the structure. In fact, here for damage state #2-L a small hairline crack occurred and for damage state #3-L this hairline cracked opened widely yielding a decrease of 12.7 and 27.6% respectively.

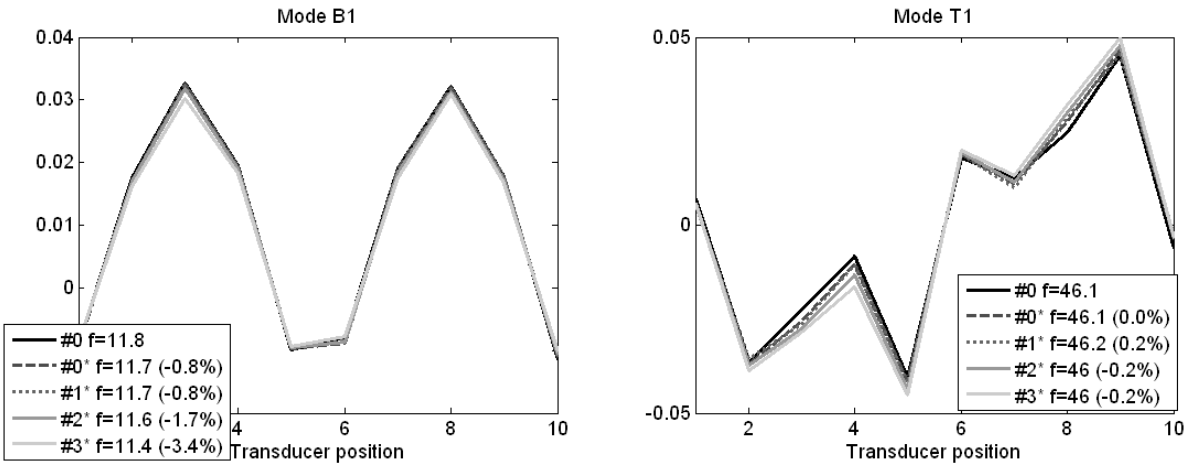

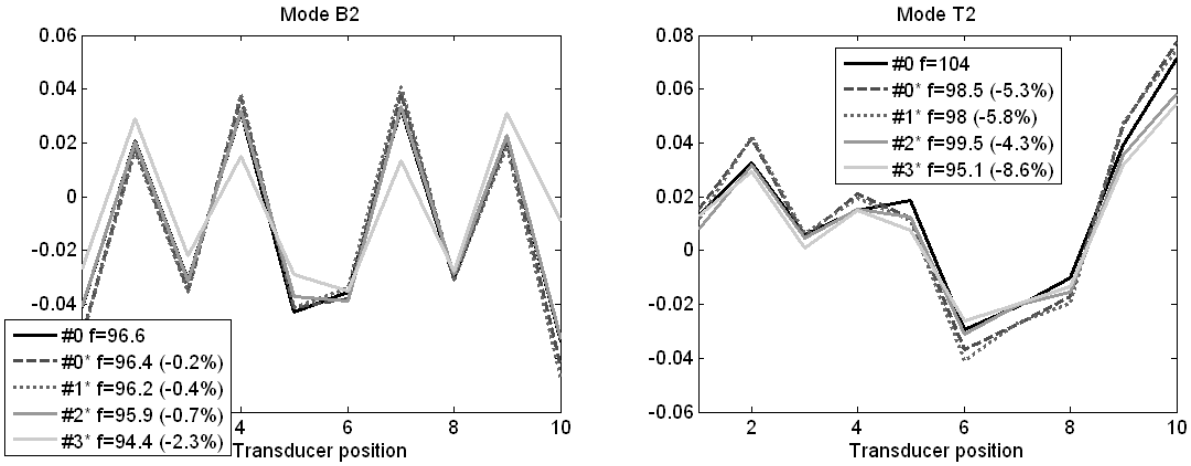

Figure 10: Eigenfrequencies and modeshapes of the unloaded prestressed slab (PC).

For Mode B2 no big changes are seen, resulting that this mode is not so affected as the first bending mode B1. Nevertheless, regarding this first mode B1 changes are obvious and correlate to the cracks in the structure, as variations of 12.7% and 27.6% are observed. Regarding the modeshapes, changes are noticed for B1 with increasing damage and for B2 not according the damage.

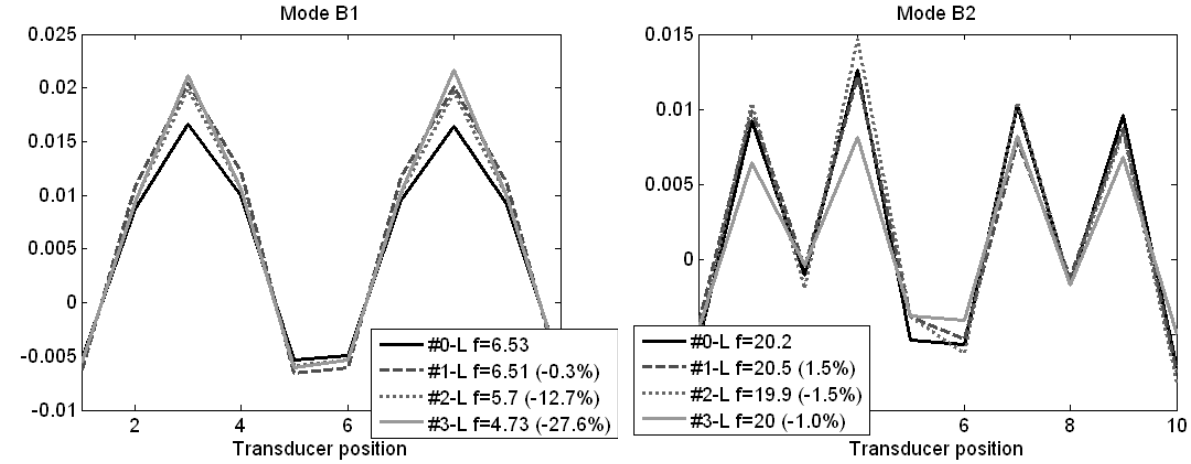

Figure 11: Eigenfrequencies and modeshapes of the prestressed slab (PC) loaded with 4 weights.

3.1.2 Bridge Champangshiehl

For the Bridge Champangshiehl, regarding the first eigenfrequency on Figure 12, one recognises a drastic decrease according the damage states. Here for damage state #1 a diminishing of 3.7% is identified compared to the intact state #0. The reason is the appearance of a first crack in the bottom plate of the bridge yielding a loss in stiffness. Further, when cutting 8 of the above tendons, i.e. 12.6% of the tendons in the top plate for this damage state #2 no decrease is retrieved, as also no crucial additional cracks are observed. Afterwards, for damage state #3 and #4, when cutting the external and 40% of the above tendons existing crack expand and more cracks occurred, marked by a decrease of the eigenfrequency by 9.9% and 15.7% for damage state #3 and #4 respectively. Further, for modes B4, T4 and T5 also big variations according the damage states are noticed, with a maximal reduction of 7.5%, 4% and 3.4% respectively.

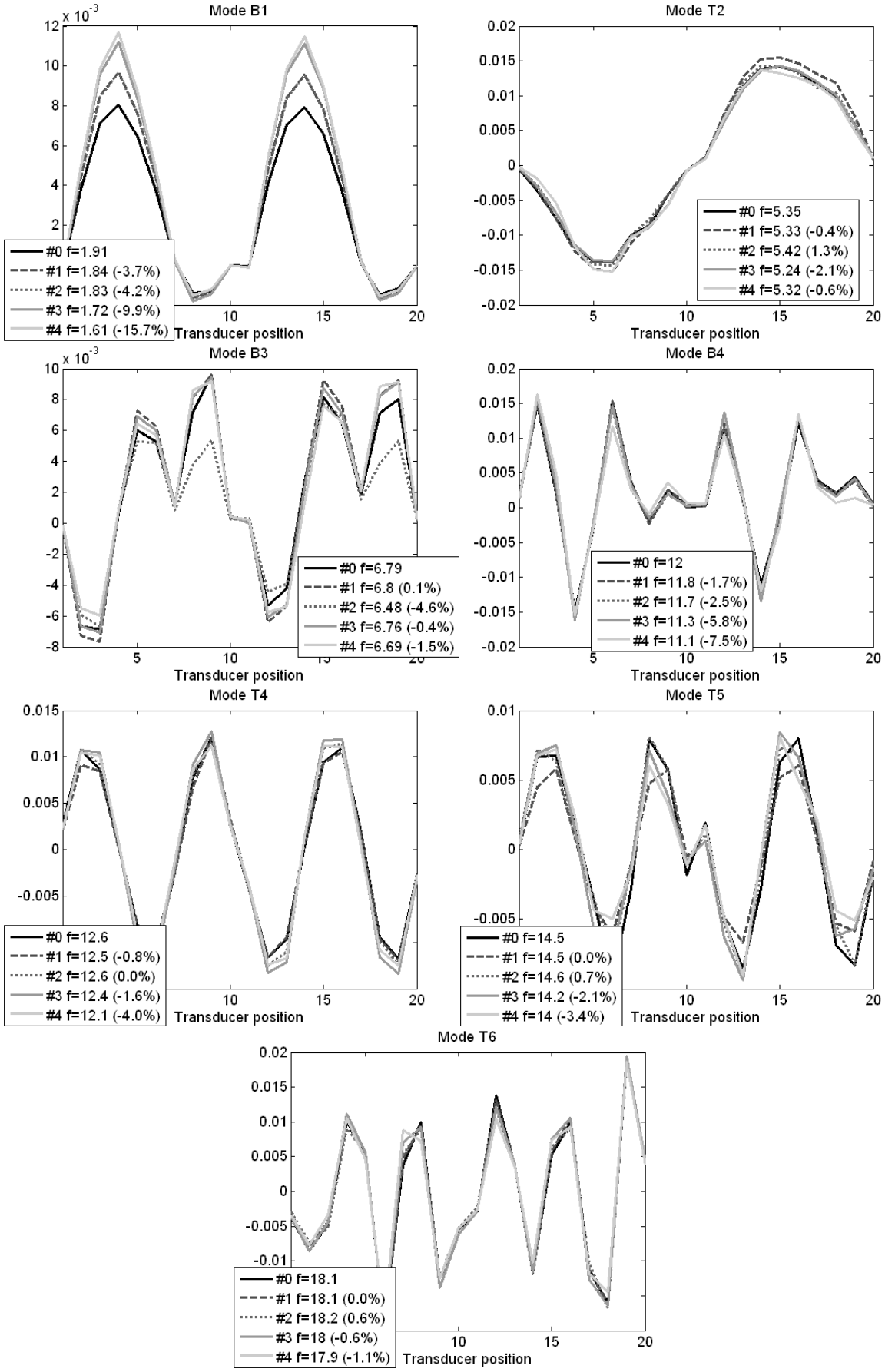

Figure 12: Eigenfrequencies and modeshapes of the Bridge Champangshiehl.

However, regarding the other modes T2, B3 and T6 no crucial changes can be observed, yielding that for the Bridge Champangshiehl a similar behaviour as for the reinforced and the loaded prestressed slab is retrieved, namely that only for some eigenfrequencies, changes according the damage can be observed revealing the occurrence of cracks in the structure. Regarding the modeshapes, only B1 seems affected by the right order of damage. Thus, as for the other modeshapes and the modeshapes presented for the slabs, the variations of the modeshapes seem not to be a good indicator for damage assessment.

3.2 Flexibility matrices

In this chapter, out of the modeshapes and the eigenfrequencies presented in the previous chapter, the flexibility matrix, which is the inverse matrix of the stiffness matrix, can be calculated. This is achieved according the following formula:

$$[K]^{-1} = \sum_{k=1}^{N} \{\Phi_k\} \cdot \frac{1}{\omega_k^2} \{\Phi_k\}^T = [F]$$

where Φ are the mass normalised modeshapes and ω the angular eigenfrequencies. Figure 13 presents an example for the flexibility matrix of the bridge Champangshiehl. On the left a 3-D plot and on the right a contour plot is shown.

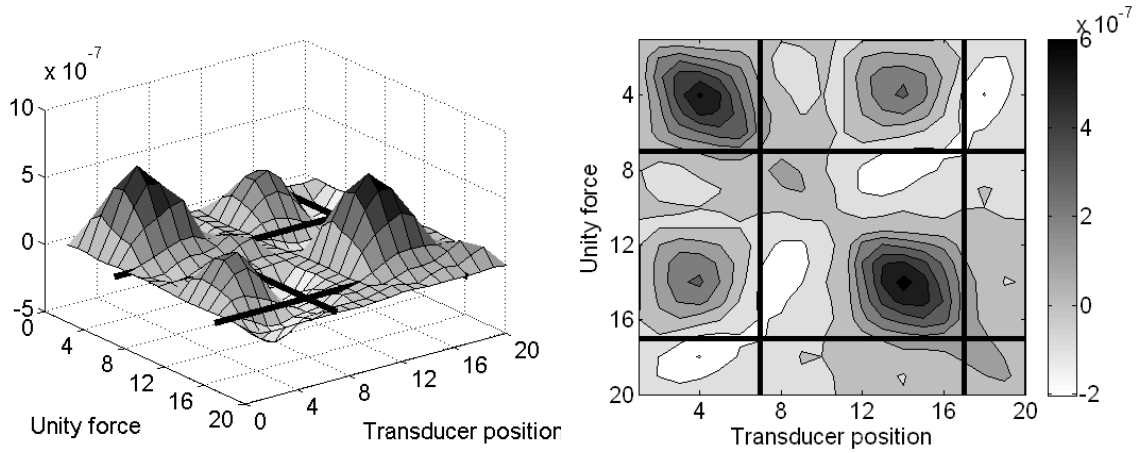

Figure 13: Flexibility matrix of the Bridge Champangshiehl for the intact state #0 as an example. The black lines represent the position of the bearing over the pylon.

Now, with these flexibility matrices for each damage state, comparisons can be made, first by plotting the diagonal elements of these matrices and second by a damage indicator proposed by Pandey et al. This one calculates the column wise maximum absolute difference of each flexibility matrix from each damage state (d) to the undamaged state (u) for comparisons [3]. First the difference of the flexibility matrices has to be calculated. Out of these ΔF matrices the maximal value δ_i for each column l is determined and plotted for each transducer position i.

$$\Delta F = |F_d - F_u| \qquad \delta_i = \max|\delta f_{li}|$$

3.2.1 Reinforced and prestressed concrete slabs

As already observed for the eigenfrequency values for the reinforced slab the changes are obvious for the last damage states, i.e. from states #1* to #3*. For damage state #0* only the excitation side is affected. In contrast, regarding the prestressed slab, only the last damage state shows clear differences to the intact state. However, these changes are small compared to the reinforced slab and the prestressed slab when loaded. This is seen regarding on the right side of the figures on the magnitude of the difference values.

For the reinforced and loaded prestressed slab, one has a magnitude of 10^{-7} and for the unloaded prestressed slab of 10^{-8}. Therefore, when the prestressed slab is loaded, the changes gets obvious, due to the opening of the cracks as already seen for the eigenfrequency values in the previous chapter.

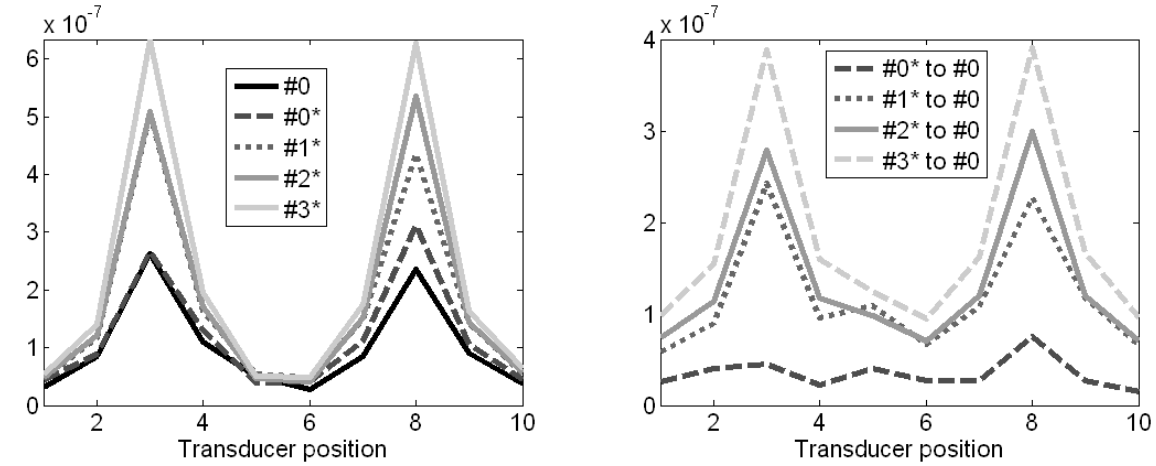

Figure 14: Diagonal elements of the flexibility matrix (left) and absolute maximal differences of the columns of the flexibility matrices (right) for the reinforced slab (RC).

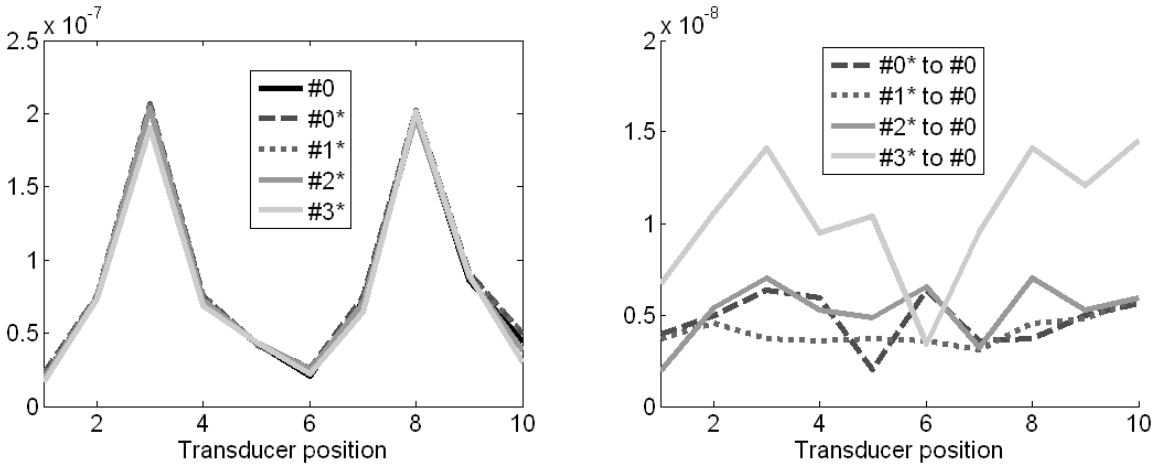

Figure 15: Diagonal elements of the flexibility matrix (left) and absolute maximal differences of the columns of the flexibility matrices (right) for the unloaded prestressed slab (PC).

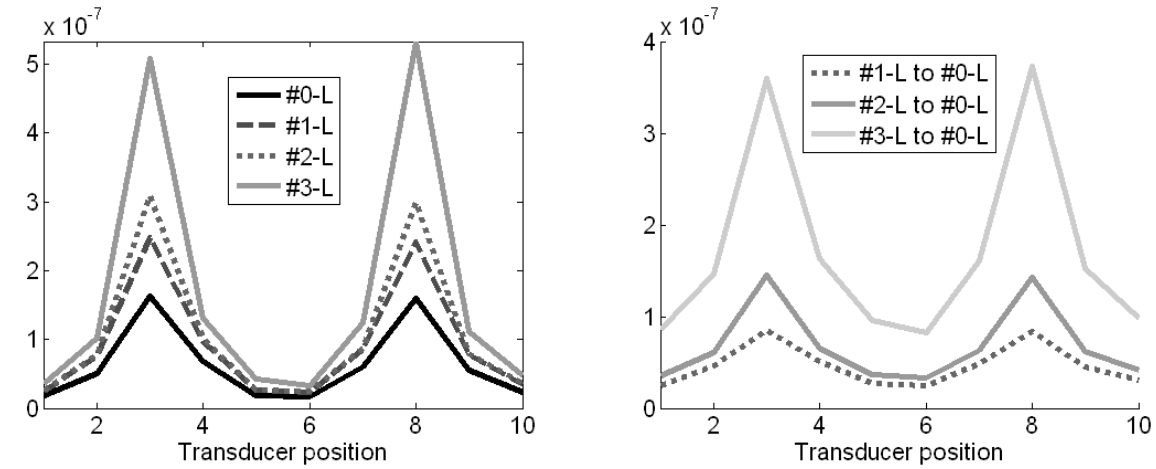

Figure 16: Diagonal elements of the flexibility matrix (left) and absolute maximal differences of the columns of the flexibility matrices (right) for the prestressed slab (PC) loaded with 4 weights.

3.2.2 Bridge Champangshiehl

For the bridge Champangshiehl, regarding the diagonal elements of the flexibility matrices and the column wise absolute difference of the flexibility matrices on Figure 17 changes are obvious. Here the localisation of the damage around the middle of the big field is clear. As damage state #2 did not consist in further changes than damage state #1, also on both figures no variations can be noticed.

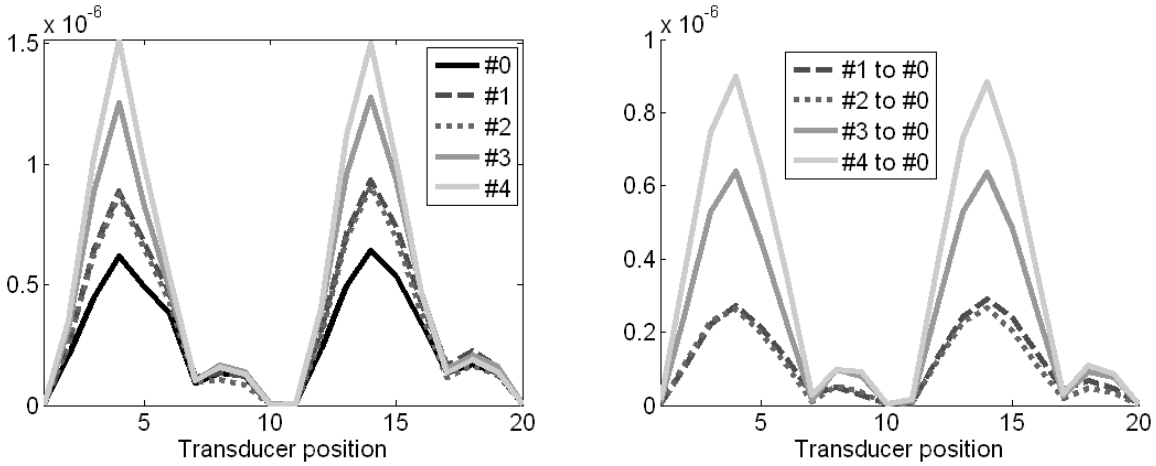

Figure 17: Diagonal elements of the flexibility matrix (left) and absolute maximal differences of the columns of the flexibility matrices (right) for the Bridge Champangshiehl

3.3 Modeshape slope and curvature methods

Another focus is put on the Modeshape slope (MSS) and curvature (MSC) method proposed by Ewins [5] and Pandey [6]. First, the slope and curvature of each modeshape has to be calculated:

$$\Phi_i^{'} = (\Phi_{i+1} - \Phi_{i-1})/2h$$

$$\Phi_i^{''} = (\Phi_{i+1} - 2\Phi_i + \Phi_{i-1})/h^2$$

with Φ the mass normalised modeshapes, h the distance between neighbour transducers and i the index of the DOFs. Here only the excited side of the bridge is considered. For each mode, the difference of slopes and the curvature for each damage state (d) to the intact state (u) are determined and summed up over all the 7 modes:

$$\left\{\Delta\Phi_i^{'}\right\} = \left|\left\{\Phi_{di}^{'}\right\} - \left\{\Phi_{ui}^{'}\right\}\right|$$

$$\left\{\Delta\Phi_i^{''}\right\} = \left|\left\{\Phi_{di}^{''}\right\} - \left\{\Phi_{ui}^{''}\right\}\right|$$

$$MSS_i = \sum_{k=1}^{7} \Delta\Phi_{ik}^{'}$$

$$MSC_i = \sum_{k=1}^{7} \Delta\Phi_{ik}^{''}$$

On Figure 18 these MSS (left) and MSC (right) parameters are plotted. One can recognise changes to the intact states for both indicators, increased for each damage state. Regarding both graphs in contrast to the analysis on the flexibility matrices, the biggest changes appear for transducers 6 and 7, and at most for damage state #4, when also the biggest changes occur on that position for the damage scenarios (cutting of 38% of the tendons and appearing of a straight lined crack in contrast to damage scenario #3). However, regarding the whole graphs, the changes are small and more difficult to interpret as for the changes in the

flexibility matrices. For example for damage state #2 changes in the MSS parameter appear on the location of the second cut, which diminishes again for #3, which is physically not explainable.

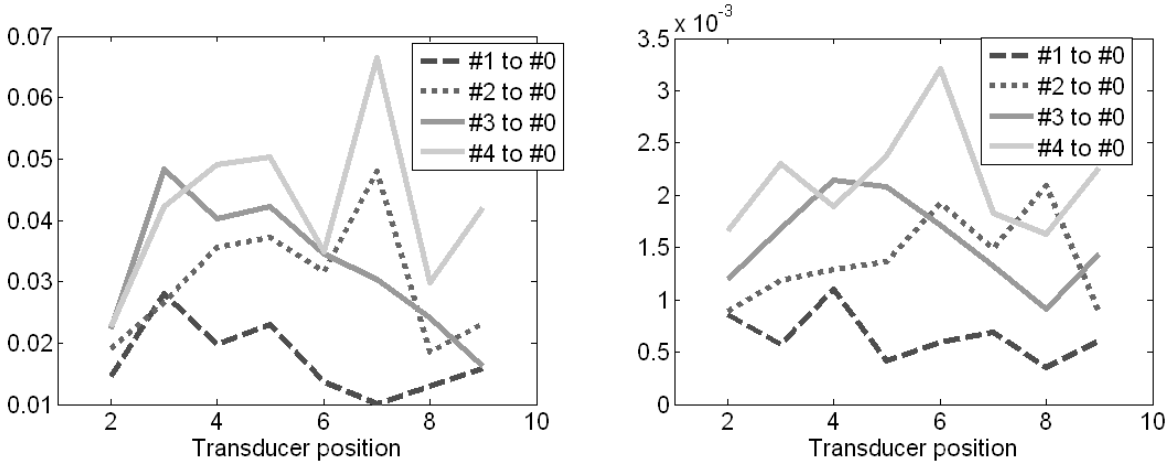

Figure 18: Sum of the differences of the slopes (MSS, left) and curvatures (MSC, right) for all the modes.

3.4 Damage indicators

In this chapter, two methods based on the slopes and curvatures are proposed. The first is by calculating the bending and the shear energy using modal parameters and the second by using the slopes and curvatures on the influence lines of the flexibility matrices for each damage state.

3.4.1 Bending and shear energy

In this paragraph, the damage indicator from Stubbs and Kim are proposed [10]. These damage indicators afterwards called by Link [8] MS and MC, present the fractional bending (curvature) and shear (slopes) energy and are determined according the following formulas:

$$MS_{ij} / MC_{ij} = \frac{(y_{d,ij}^2 / \sum_{i=1}^{N} y_{d,ij}^2 + 1)}{(y_{u,ij}^2 / \sum_{i=1}^{N} y_{u,ij}^2 + 1)}$$

$$MS_i = (\frac{1}{7}\sum_{k=1}^{7} MS_{ik} - 1) * 100$$

$$MC_i = (\frac{1}{7}\sum_{k=1}^{7} MC_{ik} - 1) * 100$$

With the variable y representing the slope Φ' and the curvature Φ'' and the index i=1-10 the number of DOFs. Also here, as for the MSS and MSC methods indications on the changes according damage can be made. For the MS parameter, changes are obvious (highest values) on transducer position 4 and 7, where also the most damage occurred. The same behaviour is recognised for the MC curves, the biggest variations are identified between transducer position 3 and 5 and for transducer position 6 and 7. However, as for the MSS and MSC parameters, one has to be cautious with the interpretation of the MS and MC values, as on the outer bearings for example also variations occur although nothing was changed.

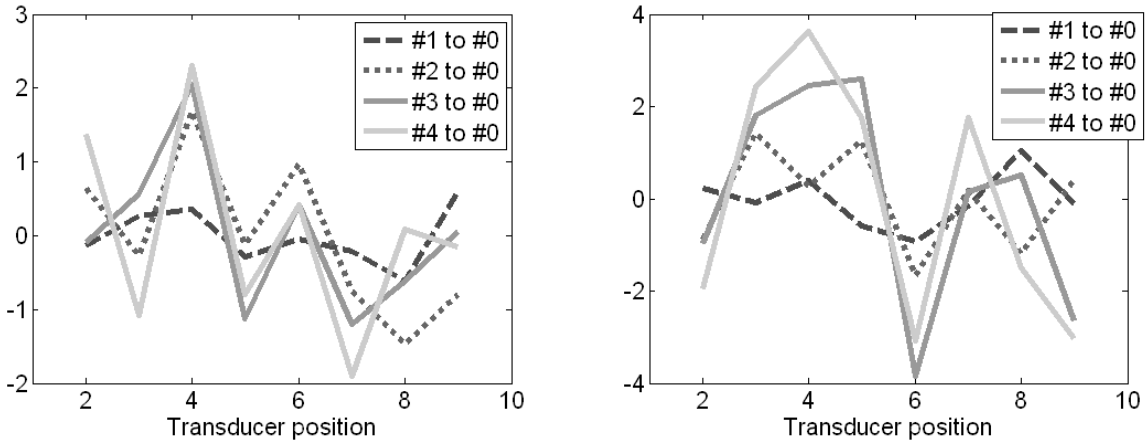

Figure 19: MS (left) and MC (right) parameters.

3.4.2 Slope and curvature of the influence line

Considering the diagonal elements F_{ii} of the flexibility matrices, which represent the influence line, meaning that for each DOF a unit force at the same DOF is applied, one can calculate the slope and curvature of this line according the following formula:

$$F_{ii}^{'} = (F_{ii+1} - F_{i-1}) / 2h$$

$$F_{ii}^{''} = (F_{ii+1} - 2F_{ii} + F_{ii}) / h^2$$

Taken the square of F'_{ii} and F''_{ii}, one can plot these values of one side of the bridge indicating the changes in the different flexibility matrices. Figure 20 presents these curves, and show clearly the position of the damage for each damage state. Regarding the curvature of the influence lines, the biggest changes occur namely at transducer position 4 in the middle of the big field and at transducer position 7 over the pylon for the last damage states.

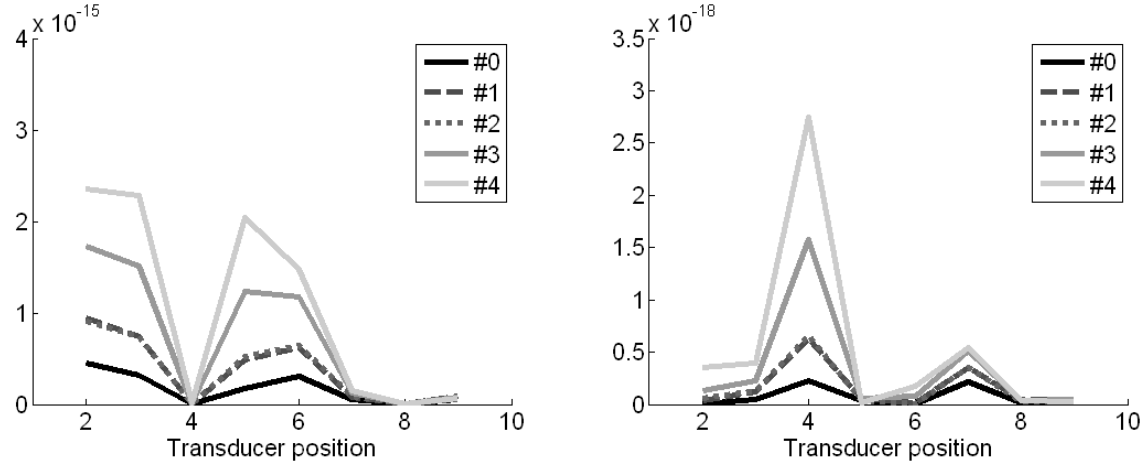

Figure 20: Slope (left) and curvature (right) of the influence line

4 Conclusion

In this paper, the dynamic testing of in situ and laboratory tests are shown. It seems that the most reliable parameters for damage identification are the changes in the eigenfrequencies and the flexibility matrices. Regarding the eigenfrequencies, damage identification is possible, as the formation of cracks, which has to

be open, is clearly identifiable by the decrease of this modal parameter. Moreover, regarding the changes in the flexibility matrices proposed by the diagonal elements, or by the column wise absolute maximal value by Pandey [3] damage localisation seems possible for the presented structures under the given severe damage. Further, regarding the other proposed methods, like the slope and curvature methods, as well as the fractional bending and shear energy damage identification is also possible, but due to the small variations, localising changes in a structure seems difficult to interpret. However, regarding again the flexibility matrices with the slope and curvature of its influence line, damage localisation is clearly manageable, as the variations to the intact state are obvious. In addition, as for the analysis of the presented methods only using a coarse grid, it appears that a large resolution of the DOF is already sufficient for damage assessment in the case of the bridge Champangshiehl. However, an appropriate number of DOF is needed calculating the slopes and curves, which was here not the case for the reinforced and prestressed slab, and, therefore, no statement of these methods including the bending and shear energy made.

References

[1] M. Waltering, D. Waldmann, S. Maas & A. Zürbes, *Untersuchung nichtlinearer Schwingungseigenschaften, zur zerstörungsfreien Zustandsprüfung am Beispiel von Stahlbetonbalken,* Beton- und Stahlbetonbau, 102, (2007), pp. 615-621

[2] J. Mahowald, V. Bungard, S. Maas, D. Waldmann, A. Zuerbes & G. De Roeck, *Comparison of linear and nonlinear static and dynamic behaviour of prestressed and non-prestressed concrete slab elements*, Proceedings ISMA 2010, Leuven, (2010), pp. 717-728

[3] A.K. Pandey & M. Biswas, *Experimental Verification of Flexiblity Difference Method for locating damage in structures,* Journal of Sound and Vibration, 184, (1995), pp. 311-328

[4] J. Mahowald, S. Maas, F. Scherbaum, D. Waldmann & A. Zuerbes, *Dynamische Methoden zur Schadensidentifikation an einer kontinuierlich geschädigten vorgespannten Zweifeldbrücke,* 4. VDI-Fachtagung Baudynamik 2012, VDI Berichte 2160, (2012), pp. 247-258

[5] Y. K. Ho & D.J. Ewins, O*n the structural damage identification with mode shapes*, Proceedings of the European COST F3 Conference on System Identification & Structural Health Monitoring, Universidad Politécnica de Madrid, Spain, (2000), pp. 677-684

[6] A.K. Pandey, M. Biswas & M. M. Samman, *Damage detection from changes in curvature mode shapes*, Journal of Sound and vibration, 142, (1991), pp. 321-332

[7] R.P.C. Sampaio, N.M.M. Maia & J.M. M. Silva, *Damage detection using the frequency-response-function curvature method, Journal of Sound and Vibration*, 226, (1999), pp. 1029-1042

[8] M. Link & M. Weiland, *Structural damage identification-Model based or not?* Proceedings of the International Conference on Structural Engineering Dynamics, Tavira, Portugal, 20-22 June (2011)

[9] Scherbaum, F. & Mahowald, J. (2011), *Report Bridge Champangshiehl 2*, University of Luxembourg, unpublished

[10] N. Stubbs, J.T. Kim & R.F. Charles, *Field verification of a non-destructive damage localization and severity estimation algorithm*, Proceedings XIII International Modal Analysis Conference, Nashville, USA, (1995), pp. 210-218